Determination of the intrinsic stress/strain equation of thin polymer films from stretching experiments under plane-strain tension

Christian G'Sell*
Laboratoire de Métallurgie Physique & Science des Matériaux (URA CNRS 155), Ecole des Mines, Parc de Saurupt, 54042 Nancy, France

and Alfredo Marquez-Lucero
Centro de Investigacion Cientifica de Yucatan, Departamento de Polímeros, Km. 7 Ant. Carr. a Progreso, Ex-Hacienda Xcumpich, Merida (Yucatan), Mexico
(Received 13 July 1992)

Thin films of amorphous poly(ethylene terephthalate) were stretched under plane-strain tension at temperatures from 20°C to 100°C and at various elongation rates. It was observed that under such a deformation regime a neck is likely to form perpendicular to the tensile axis and to propagate steadily towards the gripped ends of the sample. The kinetics of the neck propagation was recorded carefully during the course of the tests by means of a photographic technique and the profile of the neck was analysed by quantitative microscopy during the propagation stage. It is shown that, under simple assumptions, the plastic constitutive equation of the material can be determined from this procedure in terms of the local effective stress *versus* the local effective strain and effective strain-rate at each of the temperatures investigated. It is demonstrated that the method employed is generally applicable to most ductile polymers.

(Keywords: poly(ethylene terephthalate); films; plane-strain tension; necking)

INTRODUCTION

Modelling the plastic deformation of a given material under generalized straining conditions requires basically two types of information: an appropriate flow theory expressed in a tensorial form and an accurate stress/strain/strain rate equation along a particular strain path, usually uniaxial tension. In the case of solid polymers, it has been shown by several authors[1-3] that reasonable confidence could be placed in the Von Mises flow equation (or J_2 invariant flow theory), adequately modified to take into account the effects of hydrostatic pressure and structural anisotropy. On the other hand, it was shown in previous papers[4-7] that special experimental precautions should be taken to assess the stress/strain/strain rate up to large strains in polymers, because of the early development of abrupt necks in most of them. For polymers that maintain an homogeneous distribution of the solid phases under the shape of thick pieces (e.g. plates and rods), a novel tensile testing method has been developed[4,5,8], which is based on the *in situ* determination of the *local* stress and strain in the centre of the neck by means of a computer-aided video extensometer and on the real-time control of the local strain rate. By means of such a technique, the stress/strain/strain rate equation of the polymer is readily attainable, at constant pressure, at any temperature in the following form:

$$\sigma_e = \sigma_e(\varepsilon_e, \dot{\varepsilon}_e, T, S) \quad (1)$$

where the effective quantities σ_e, $\dot{\varepsilon}_e$ correspond to the case of uniaxial tension and represent the true mechanical state of a given material element, T is the temperature, and S is a parameter that should be adapted to take account of the current structural features of the material (orientation, crystallization, etc.).

Although the latter technique proved to be reliable for bulk specimens, it does not apply to the particular case of thin polymeric films or slices (typically thinner than 1 mm) which are commonly prepared by extrusion, microtomic cutting or evaporation. When such films are stretched in simple tension, it is well known that necks usually appear in a complex and unpredictable manner (often from the gripped ends) and then propagate over the whole surface of the sample provided an early rupture does not occur from original flaws. In any case, it is incorrect to derive any kind of constitutive equation from the recorded load/extension data since they represent the average stress and strain imposed on the film sample, but not the local stress and strain experienced by a material element.

The main objective of the present work was to overcome the above limitations by means of a novel approach applicable to polymer films when necking occurs. It is based on an experimental plane-strain tension

* To whom correspondence should be addressed

0032-3861/93/132740-10

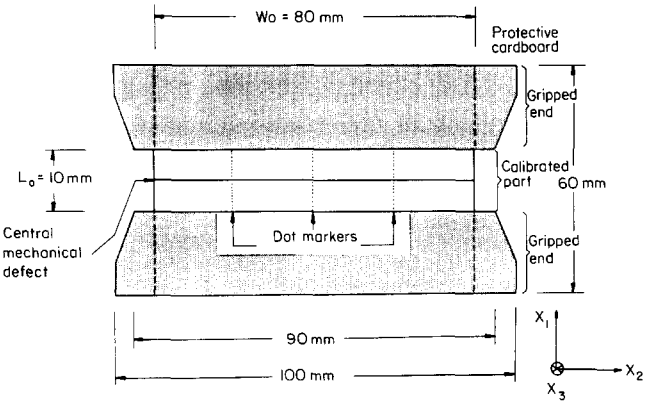

Figure 1 Geometry of the PET film specimens used

procedure and on the quantitative observation of the shoulders of the propagation neck. The analysis takes into consideration the three-dimensional stress/strain effects in the neck by means of a modified Bridgman triaxiality factor[9]. The method was applied to poly(ethylene terephthalate) (PET) at various temperatures. Effective stress/strain curves were derived for different effective strain rates. We will examine first the specific procedure employed in this work and then describe the results obtained with the PET films. The limitations of the method and its potentialities will then be analysed.

EXPERIMENTAL

Specimen preparation and characterization

A thin film of PET was obtained from the Rhone-Poulenc company (Saint-Maurice de Beynost, France). The material (ref. AK30) was extruded from the melt through a slit die and quenched on a chilled roll to obtain an amorphous structure. The thickness of the film was $h_0 = 155\ \mu m$. It was optically transparent and free from visible defects. The weight-average molecular weight, $\bar{M}_w$, of the PET was $\simeq 40\,000\ g\ mol^{-1}$, with a degree of polydispersity of ≈ 2. For optimum surface conditions in the industrial process, 300 ppm of fine kaolinite particles were added to the polymer.

The index of crystallinity X_v (crystalline volume fraction) was determined by means of a density gradient column filled with a sodium bromide solution at 23°C. The results were interpreted according to a two-phase model[10] which takes into account the crystal density $\rho_c = 1.455\ g\ cm^{-3}$ and the amorphous density $\rho_a = 1.355\ g\ cm^{-3}$ following the equation $X_v = (\rho - \rho_a)/(\rho_c - \rho_a)$, where ρ represents the sample density. By this technique, the initial density of the undeformed PET film was found to be equal to $\rho = 1.338 \pm 0.001\ g\ cm^{-3}$, corresponding to an essentially amorphous structure ($X_v < 2\%$).

Chain orientation was also investigated through birefringence measurements. The birefringence Δn was obtained by using a 30-order Berek compensator under white light (mean wavelength = 550 nm). It was found that the initial film was isotropic with a birefringence lower than the precision of the technique ($\Delta n = 0.0 \pm 0.001$).

Tensile specimens were cut from PET film in the shape depicted in *Figure 1* with a calibrated length $L_0 = 10$ mm, much shorter than the width $W_0 = 80$ mm. The upper and lower parts of the sample, protected by cardboard sheets, serve to be tightened in the grips of the tensile machine. The particular geometry of the samples was chosen in order to impose a plane-strain extension, since the confinement of the deformation in the relatively short length prevents the width from shrinking significantly during the stretching, as will be verified later. The specimens were marked with three rows of fine dots parallel to the tensile axis (by means of a dry transfer marking technique) in order to follow the distribution of strains under stretching from the relative displacement of the dots. For this purpose, the specimen was photographed periodically during the tests by means of an Olympus camera. In order to control the initiation of the neck, a predeformation defect was introduced centrally in each specimen by folding and defolding the film locally. It was shown in a previous paper[11] that such a 'mechanical' defect acts as an efficient neck initiator in those cases where a neck is likely to be formed.

Tensile testing procedure

The tests were carried out with an Instron 8032 servo-hydraulic tensile machine equipped with a computerized controller. In addition to this conventional equipment, a new environmental chamber was designed for the present study (*Figure 2*). It is able (i) to heat the film samples from ambient to 100°C within less than 200 s, (ii) to stabilize the temperature in time and space with a precision greater than 1°C and (iii) to allow the *in situ* observation of the specimens during the stretching. The chamber is equipped with front and rear windows. Fast heating is obtained by blowing hot air directly on the sample from two turbines situated on both sides. A high-rate temperature controller adjusts the heat flow continuously in response to very fine thermocouples situated near both edges of the sample.

Eight different test temperatures were chosen from 20 to 100°C and, at each temperature, eight elongation rates

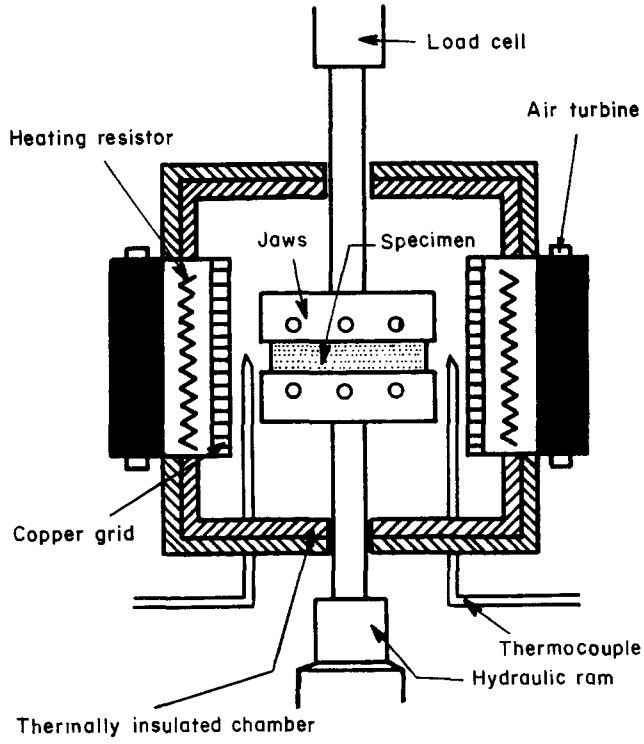

Figure 2 General diagram of the temperature-controlled plane-strain tensile system

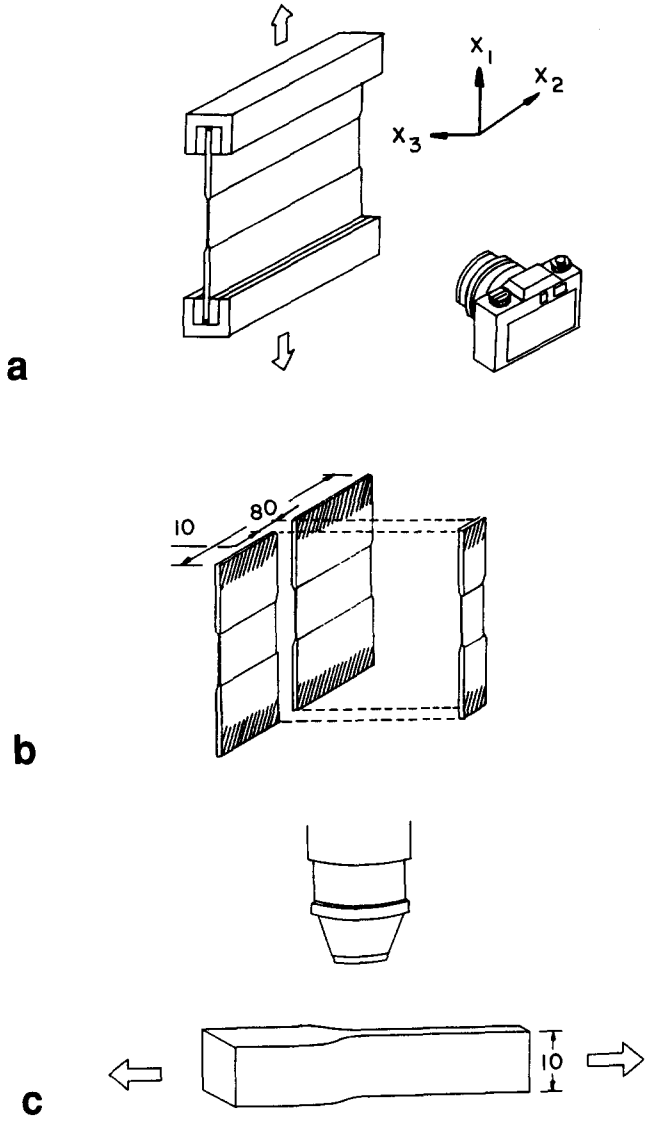

Figure 3 Diagrammatic schedule of the testing procedure. (a) Front-view photography during the test. (b) Cutting out of a longitudinal strip 10 mm wide from the centre of the specimen, at −70°C. (c) Microphotography of the transverse section of the strip

$\dot{L}(=dL/dt)$ from 3×10^{-3} to 3×10^{-1} mm s^{-1}, were performed.

The general testing procedure was as follows:

1. The specimen was gripped and a first photograph was immediately taken.
2. The specimen was preheated for 5 min and photographed a second time.
3. The extension was started, the load/extension curve being recorded while taking a series of photographs (*Figure 3a*).
4. The extension was stopped at an elongation of 20 mm. The specimen was immediately quenched in cold air. Thereafter it was removed from the tensile machine.
5. The specimen was subsequently cooled to −70°C.
6. A longitudinal band of 10 mm width was carefully cut from the specimen equidistant from its edges while it was still at −70°C (*Figure 3b*).
7. The transverse section of this band was observed with a microphotographic camera, the band being in a miniaturized tensile jig under a nominal stress slightly lower than the stress recorded when the test was stopped (*Figure 3c*).
8. The microphotographs of this transverse section were subsequently analysed in order to determine the thickness profile of the band quantitatively.

RESULTS

Slow tensile tests under T_g

The four diagrams in *Figure 4* were obtained sequentially with a PET film specimen stretched at a rate of 5×10^{-2} mm s^{-1} at a temperature of 20 ± 1°C. *Figure 4a* shows the specimen mounted in the jaws of the tensile machine before starting the test. The white central region is the calibrated zone. The grips are represented in black above and below. The horizontal line is the mechanical defect. *Figures 4b–d* show the specimen at three values of the stretching ratio $\lambda=L/L_0$ equal to 1.5, 2.0 and 3.0, respectively. It is observed that a central band appears at the mechanical defect and spreads along the specimen, while stretching proceeds. In this zone, the mechanical

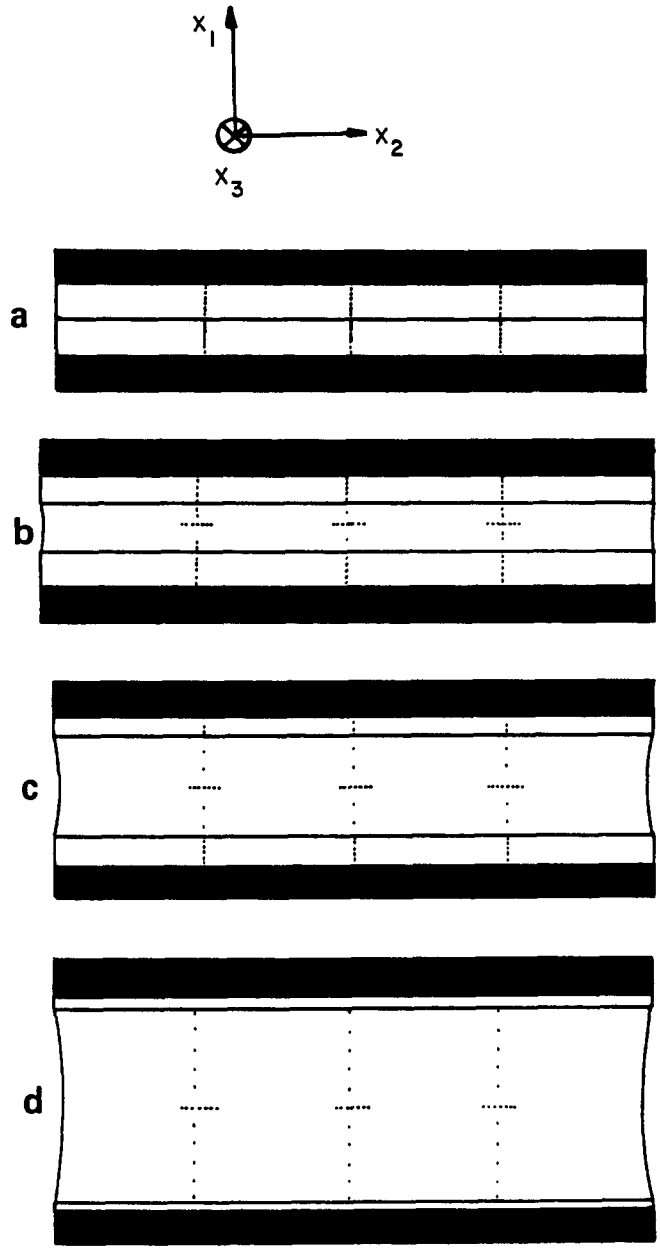

Figure 4 Stretching of a PET film specimen at 20°C and an elongation rate of 5×10^{-2} mm s^{-1}. Initial specimen dimensions (a): $L_0=10$ mm, $W_0=80$ mm, $h=155$ μm. Stretching ratio $\lambda(=L/L_0)$: (b) 1.5; (c) 2.0; (d) 3.0

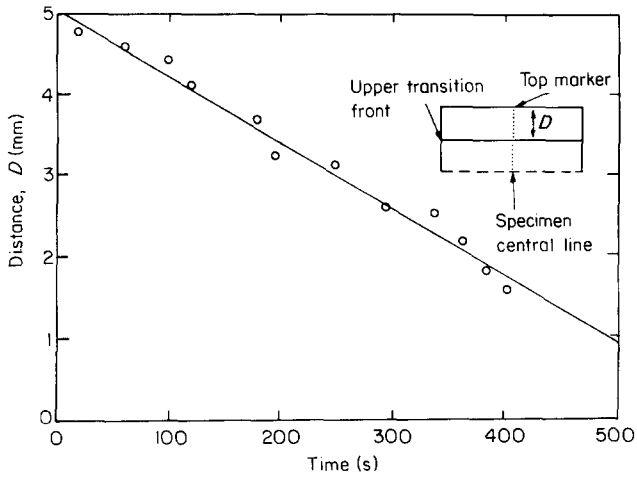

Figure 5 Distance between the upper transition front and the top marker as a function of time under the same conditions as in *Figure 4*. The plane-strain propagation speed of the neck, v_p, (8.23×10^{-3} mm s^{-1}) is given by the slope of the linear regression line

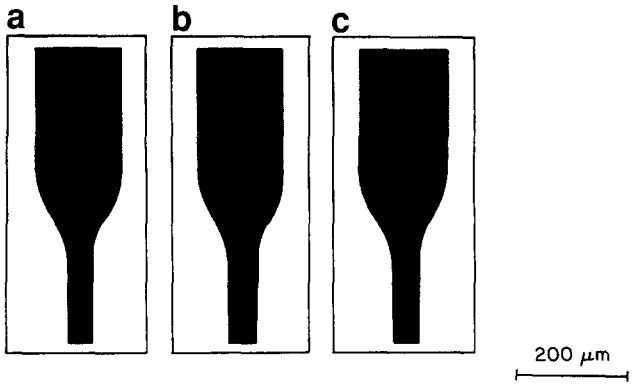

Figure 6 Transverse sections of the three different film specimens, tested under the same conditions as in *Figure 4*, for three values of the stretching ratio λ: (a) 1.5; (b) 2.0; (c) 3.0

markers are separated by a distance several times higher than in the rest of the specimen, corresponding therefore to a necking process. Since the vertical marker rows remain straight and equidistant, the band actually constitutes a 'plane-strain neck' (according to a term used in an earlier work[12]) and the two horizontal lines limiting this region are its 'transition fronts'[13].

The distance between the upper transition front and the top marker is displayed in *Figure 5* as a function of time. It appears that the propagation speed v_p of this front is practically constant. It was verified that the lower transition front propagates at the same constant speed downward. In addition, three transverse sections of the upper transition front are shown in *Figure 6* for specimens tested under the same conditions as previously for up to three different values of the stretching ratio λ. One notes that the thickness in the neck region is approximately one-third of the original value, and that the size of the transition front is similar to the thickness of the unnecked region. Lastly, it is remarkable that the geometry of the front is the same for these three profiles. In consequence it is stated that the plane-strain neck propagates under steady-state conditions in the PET films.

The curve in *Figure 7* displays the variation of the nominal stress $\sigma_n = F/(h_0 W_0)$ *versus* the stretching ratio λ during the previous test of *Figure 4*. It shows an initial quasi-linear viscoelastic stage, followed by a very short yield transition and an extended plateau corresponding to plane-strain neck propagation. It is interesting to note in this case that the load does not exhibit any drop at yield, in contrast to specimens free of mechanical defect[14,15]. This is because the mechanical defect which was introduced before the test acts as a built-in plane-strain neck and bypasses the excess load normally required for the initiation of the plastic instability. The above mechanical behaviour, characterized by a highly inhomogeneous stretching, is typical of all the PET specimens tested at temperatures below the glass transition temperature ($T_g \simeq 70$°C). It will be ascribed to 'plane-strain cold-drawing behaviour'.

Slow tensile tests above T_g

In addition to the matter above, *Figure 8* shows detailed views of a specimen stretched at 100°C, for the same elongation rate as the previous test (5×10^{-2} mm s^{-1}). As stretching proceeds, it is noted that the marker rows remain straight, which shows that the plane-strain assumption is valid again here. In contrast to the glassy state, it is now evident from the distance between individual markers that the deformation is much more homogeneous and that there is no longer a transition front. Even though the inter-marker distance increases more near the median cross-section of the specimen than at the upper and lower ends, the change is limited and very progressive (it is probably due to a small temperature gradient between the specimen and the grips).

Finally, it is found in *Figure 9* that the nominal stress at 100°C is typically one hundred times smaller than the corresponding value at 20°C. Furthermore, the shape of the σ_n *versus* λ curve is very different. An initially parabolic viscoplastic regime is observed up to $\lambda \simeq 1.5$, after which the nominal stress decreases gradually as the sample becomes thinner.

The above behaviour, typical of all the specimens stretched slowly between the glass transition (T_g) and the melting point (T_m) is ascribed to the 'plane-strain hot-drawing behaviour'.

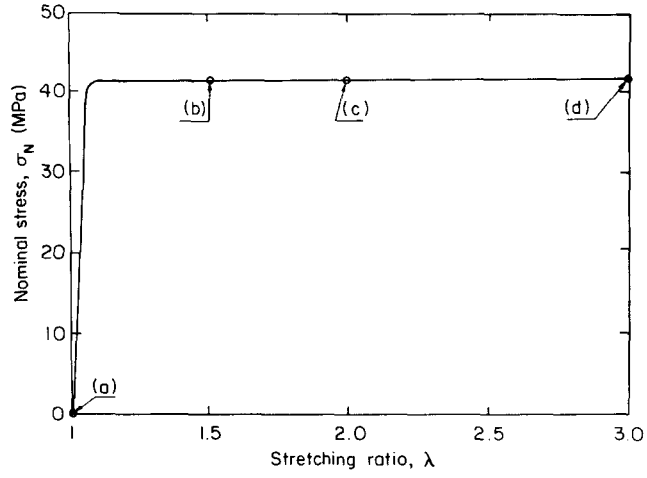

Figure 7 Nominal stress σ_N *versus* stretching ratio λ for the specimen in *Figure 4*

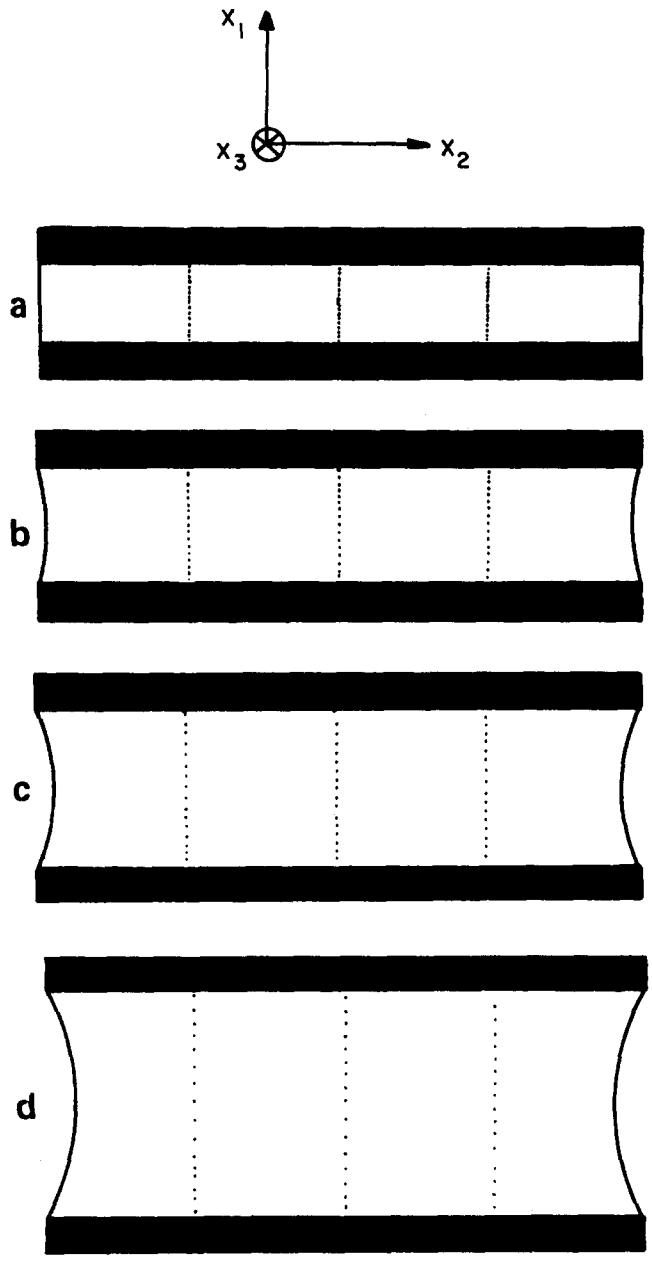

Figure 8 Stretching of a PET film specimen at 100°C, and an elongation rate of $5\times10^{-2}\,\mathrm{mm\,s^{-1}}$. Initial specimen dimensions (a): $L_0=10\,\mathrm{mm}$, $W_0=80\,\mathrm{mm}$, $h_0=155\,\mu\mathrm{m}$. Stretching ratio $\lambda(=L/L_0)$: (b) 1.5; (c) 2.0; (d) 3.0

DETERMINATION OF THE EFFECTIVE STRESS/STRAIN RESPONSE

As mentioned previously, the method developed here is based on a modified long-wavelength analysis[7] that takes into consideration the three-dimensional effects using a Bridgman triaxiality correction factor[9]. In this analysis, the material is assumed to be incompressible and isotropic and to deform isothermally.

In the following section, we will present in five successive steps how the experimental data can be exploited to obtain the effective stress/strain behaviour of the material. This method will be based not only on the nominal stress/stretch curves recorded during the tests, but also the local distribution of strains determined from the front and transverse microphotographic analyses.

Local measurement of the axial stress, strain and strain rate

The axial components of stress (σ_{11}), strain (ε_{11}) and strain rate ($\dot{\varepsilon}_{11}$) were measured at two points: (i) in the centre of the sample for all the specimens and, (ii) in the transition front for the specimens exhibiting a plane-strain cold-drawing behaviour.

At the centre of the sample, the axial strain component (ε_{11}) is defined as

$$\varepsilon_{11}=\ln(l/l_0) \tag{2}$$

where l_0 and l are the initial and current intermarker distances measured at the central markers on the front photographs under load. In the same zone, the axial stress component (σ_{11}) is given by the Kirchoff stress

$$\sigma_{11}=(F/A_0)\exp(\varepsilon_{11}) \tag{3}$$

where F is the current load and $A_0=h_0W_0$ the initial cross-section. The axial strain-rate component ($\dot{\varepsilon}_{11}$) is obtained by a polynomial multiple regression of the experimental data of the axial strain ε_{11} *versus* time (each value of $\dot{\varepsilon}_{11}$ determined from a polynomial fitted from five data points).

On the other hand, in the transition front, the axial stress, strain and strain-rate components are determined following the procedure outlined below:

1. On a transverse photograph similar to those shown in *Figure 6*, the film thickness, h, is measured at fifty cross-sections 8 μm apart along the transition front. A typical $h(x_1)$ curve is displayed in *Figure 10a* as a function of the axial coordinate x_1.
2. The axial strain component ε_{11} in each cross-section is derived from the relation:

$$\varepsilon_{11}(x_1)=\ln[h_0/h(x_1)] \tag{4}$$

where h_0 is the initial specimen thickness.

3. The axial stress component σ_{11} in the corresponding cross-section is obtained by the equation:

$$\sigma_{11}(x_1)=F_p/A(x_1)=[F_p/A_0(x_1)]\exp[\varepsilon_{11}(x_1)] \tag{5}$$

where F_p is the drawing load in the plateau stage, more particularly at a stretching ratio $\lambda=3.0$.

4. In order to measure the axial strain-rate component $\dot{\varepsilon}_{11}$, a procedure prompted by the work of Hutchinson and Neale[13] is used. This procedure is based on the observation that the slope of the transition front

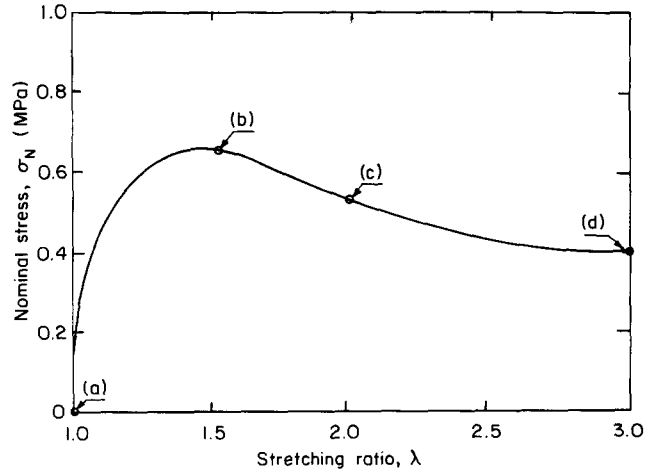

Figure 9 Nominal stress σ_N *versus* stretching ratio λ for the specimen in *Figure 8*

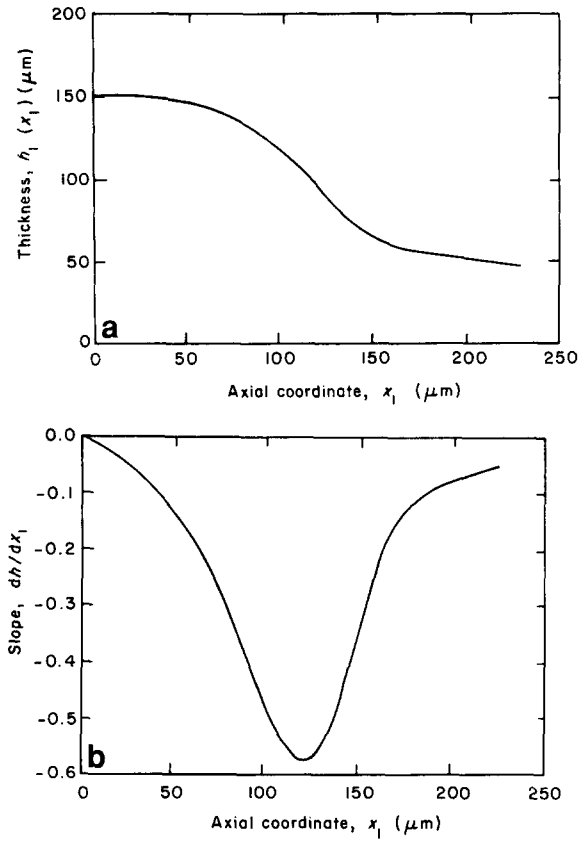

Figure 10 (a) Thickness profile $h(x_1)$ for the same conditions as in *Figure 4*, at a stretching ratio $\lambda = 3$. (b) Slope of the thickness profile (dt/dx_1)

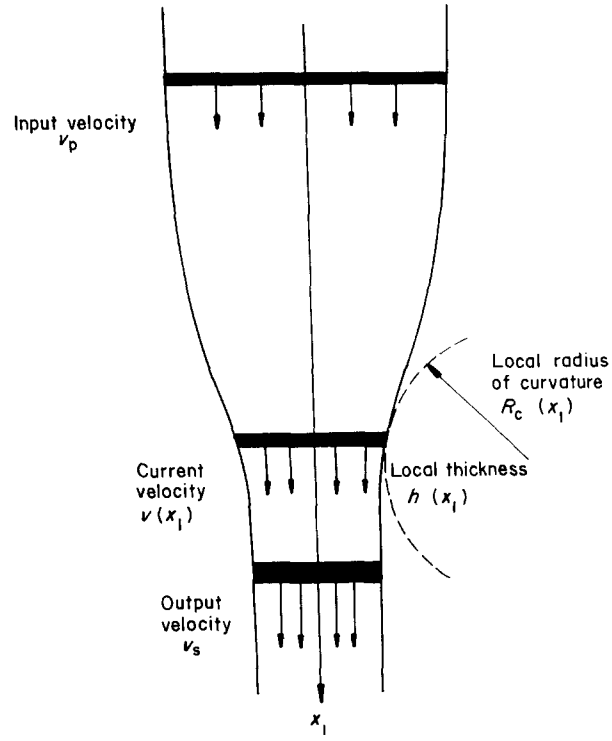

Figure 11 Kinematics of the polymer flow into an immaterial die, equivalent to the steady-state neck propagation in a film (after Hutchinson and Neale[13])

(*Figure 11*) is invariable during the propagation of the neck in the cold-drawing plane-strain behaviour once the steady-state propagation condition is reached. By considering a coordinate frame which is translating with the front, the latter can be seen as an ideal immaterial die through which the material flows from the unnecked toward the necked region. In reference to this frame, the velocity $v(x_1)$ of a given cross-section can be obtained from:

$$v(x_1) = v_p \exp[\varepsilon_{11}(x_1) - \varepsilon_{11u}] \tag{6}$$

where v_p is the propagation speed of the transition front and ε_{11u} is the axial strain component in the unnecked zone. Under the assumption of a steady-state propagation, it was shown in a previous paper[7] that the local strain-rate component $\dot{\varepsilon}_{11}$ can be derived from the cross-sectional gradient through the following relation (*Figure 11*):

$$\dot{\varepsilon}_{11}(x_1) = \frac{d\varepsilon_{11}}{dx_1} v(x_1) = -\frac{v_p \exp[\varepsilon_{11}(x_1) - \varepsilon_{11u}]}{h(x_1)} \left[\frac{dh(x_1)}{dx_1}\right] x_1 \tag{7}$$

where dh/dx_1 is the local slope of the $h(x_1)$ curve. It is displayed in *Figure 10b versus* the axial coordinate x_1.

The curves $\sigma_{11}(\varepsilon_{11})$ and $\dot{\varepsilon}(\varepsilon_{11})$ obtained with the above methods are shown in *Figure 12*, for the tests performed at 20 and 100°C. The curves at 100°C were determined using the measurements at the centre of the specimen, while the curves at 20°C were determined from the measurements at the transition front.

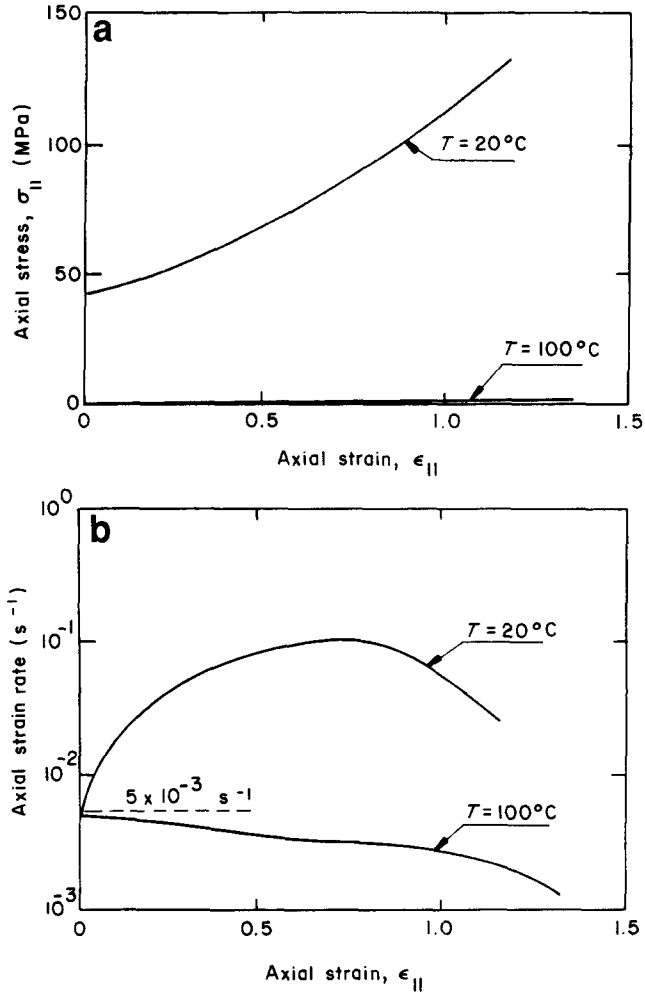

Figure 12 Determination of the axial variables for the tests at 20°C and 100°C ($\dot{L} = 5 \times 10^{-2}$ mm s^{-1}). (a) Axial stress/strain curves. (b) Axial strain rate/strain curves

Determination of the effective stress, strain and strain rate

In order to determine the effective stress (σ_e), strain (ε_e) and strain rate ($\dot{\varepsilon}_e$), we have utilized the J_2 flow theory. Although this approach is not necessarily a rigorous model for polymers, it has been frequently used to represent their multiaxial behaviour[1-3,12,15]. In this theory, the effective (uniaxial) parameters are linked to the multiaxial variables by the following relations:

$$\varepsilon_e = (2/3 \quad \varepsilon_{ij} \quad \varepsilon_{ij})^{1/2}$$
$$\dot{\varepsilon}_e = (2/3 \quad \dot{\varepsilon}_{ij} \quad \dot{\varepsilon}_{ij})^{1/2}$$
$$\sigma_e = (3/2 \quad S_{ij} \quad S_{ij})^{1/2} \qquad (8)$$

where ε_{ij}, $\dot{\varepsilon}_{ij}$ and S_{ij} are the strain, strain-rate and deviatoric stress tensors of the multiaxial field, respectively.

The determination procedure which follows is divided in two steps: the first takes into account the constant width and small thickness of the film, and the second introduces the perturbation caused by the presence of a neck. For practical reasons, the parameters obtained in the first step are referred to as 'equivalent' stress, strain and strain rate, and the variables resulting from the second step are referred to as 'effective'.

First step. The deformation mode in the above tests can be regarded to obey both plane strain (constant width) and plane stress (small thickness) conditions. Using equations (8), the equivalent strain, strain rate and stress are then given by:

$$\varepsilon_{eq} = 2/\sqrt{3}\varepsilon_{11}, \quad \dot{\varepsilon}_{eq} = 2/\sqrt{3}\dot{\varepsilon}_{11}, \quad \sigma_{eq} = \sqrt{3}/2\sigma_{11} \qquad (9)$$

Therefore, it should be noted that the 'equivalent' curves $\sigma_{eq}(\varepsilon_{eq})$ and $\dot{\varepsilon}_{eq}(\varepsilon_{eq})$ are obtained from the curves in *Figure 12* by merely applying the normalizing factors $2/\sqrt{3}$ and $\sqrt{3}/2$.

Second step. In several numerical studies on the plastic instabilities in polymers[12,16], it was shown that the complex geometry of the neck introduces a significant perturbation in the stress field, while the local strain field perturbation is of minor importance. It may thus be written:

$$\varepsilon_e \simeq \varepsilon_{eq} \quad \dot{\varepsilon}_e \simeq \dot{\varepsilon}_{eq} \quad \sigma_e(x_1) = F_T(x_1)\sigma_{eq}(x_1) \qquad (10)$$

where F_T is the 'stress triaxiality factor'. An exact expression of this factor is not rigorously available because, in principle, the stress field in the neck depends not only on its geometry, but also on the mechanical properties of the material[13,17,18]. Nevertheless, in the particular case of an axisymmetric tensile specimen, it has been demonstrated in previous papers[7,19] that the stress triaxiality factor is approximated with very good precision by the model of Bridgman[9,20], which involves geometric parameters only. The same approach is applicable to the plane strain necks. For a concave curvature, this stress triaxiality factor is then given by:

$$F_T(x_1) = \left\{\left[1-\frac{4}{N_c}\right]^{1/2} \ln\left[1+\frac{N_c}{2} + \left\{N_c\left(1+\frac{N_c}{4}\right)\right\}^{1/2}\right] - 1\right\}^{-1} \qquad (11)$$

$$N_c = h(x_1)/R_c(x_1)$$

where R_c is the radius of curvature of the specimen profile and N_c is the reduced curvature ratio. For a convex curvature, it becomes:

$$F_T(x_1) = \left\{2\left[\mathrm{abs}\left(1-\frac{4}{N_c}\right)\right]^{1/2} \times \tan^{-1}\left[\left[\mathrm{abs}\left(1-\frac{4}{N_c}\right)\right]^{-1/2}\right] - 1\right\}^{-1} \qquad (12)$$

The variations of the F_T factor are displayed in *Figure 13* as a function of the reduced curvature ratio N_c. It should be noted that this factor is greater than 1 for the convex curvatures ($R_c < 0$), and lower than 1 in the concave regions ($R_c > 0$).

In *Figure 14*, we have plotted the N_c ratio and the corresponding triaxiality factor F_T as a function of the axial coordinate x_1 in the typical case of a PET film stretched at room temperature. It is noted that the perturbation expressed by the triaxiality factor reaches about +20% and −10% in the cross-section of maximum and minimum curvature, respectively.

In *Figure 15*, the effective stress/strain curve obtained by applying the previous factor is compared with the equivalent stress/strain curve and the axial stress/strain curve for a temperature of 20°C and an elongation rate of 5×10^{-2} mm s^{-1}.

Evaluation of the strain-rate sensitivity coefficient

The strain-rate sensitivity coefficient is classically defined by the following equation:

$$m = \left[\frac{\partial \ln \sigma_e}{\partial \ln \dot{\varepsilon}_e}\right]_{\varepsilon_e, T, P} \qquad (13)$$

It has been evaluated, for each temperature, by a linear regression on experimental $\ln(\sigma_e)$ *versus* $\ln(\dot{\varepsilon}_e)$ plots similar to those illustrated in *Figure 16* for different values of ε_e at 20°C. Since the strain sensitivity coefficient, m, presents some minor variations with ε_e, we will consider here its average value $\bar{m}$ for simplicity.

It is seen in *Figure 17* that this latter coefficient ($\bar{m}$) increases continuously with temperature. In particular, it undergoes an abrupt rise in the range of the glass-transition temperature.

Determination of the effective stress/strain behaviour for a reference strain rate

In a preceding section, the effective stress/strain curves have been determined for the particular strain-rate path

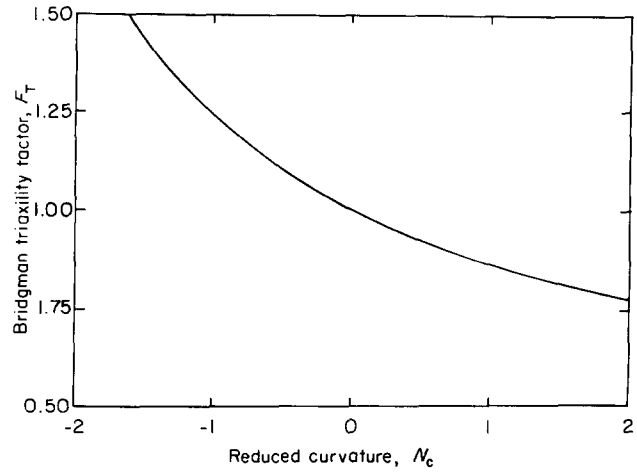

Figure 13 Influence of the reduced curvature, $N_c(=t/R_c)$ of the cross-section profile on the stress triaxiality factor in plane-strain tension (after Bridgman[9])

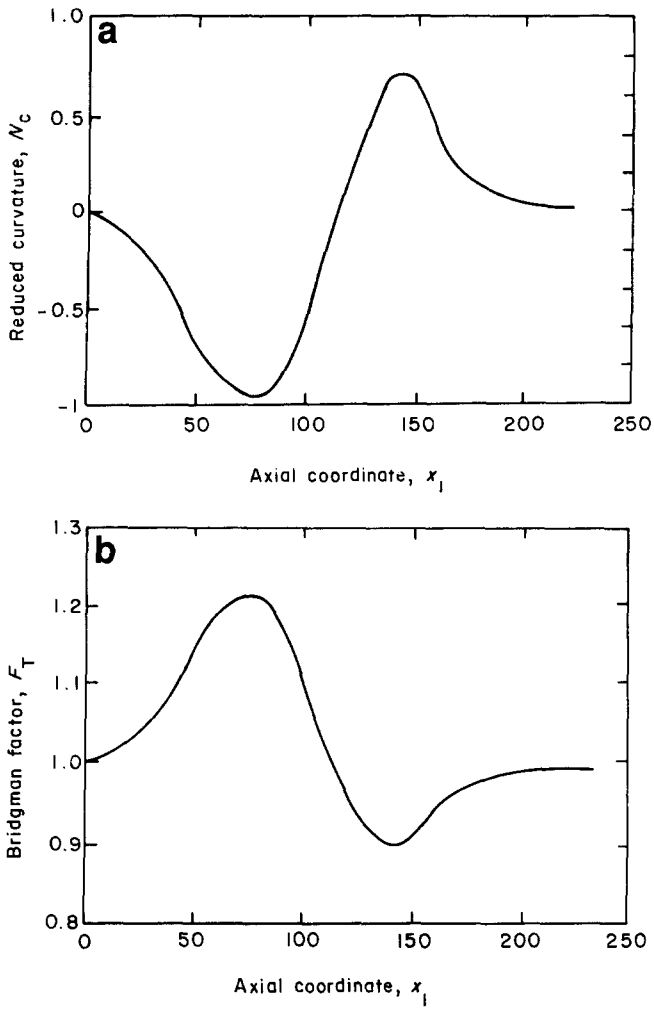

Figure 14 Assessment of the stress triaxiality effect for the same testing conditions as in *Figure 4*. (a) Reduced curvature $N_c(=t/R_c)$ along the axial coordinate. (b) Stress triaxiality factor F_T along the axial coordinate

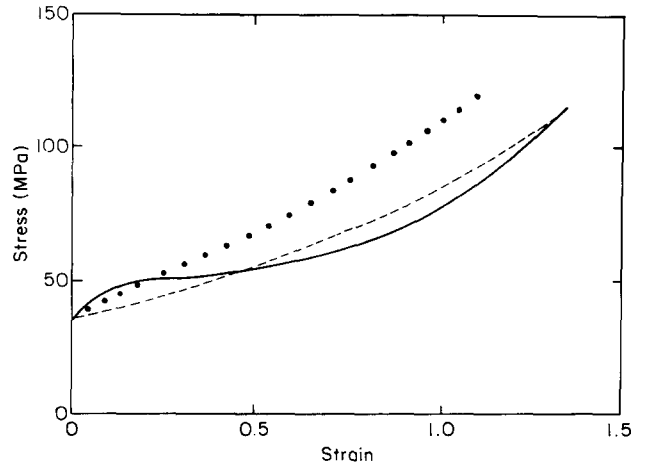

Figure 15 Determination of the effective stress/strain curve ($\sigma_e(\varepsilon_e)$) (——) of the PET for the same testing conditions as in *Figure 4*. The equivalent ($\sigma_{eq}(\varepsilon_{eq})$) (– – – –) and nominal ($\sigma_{11}(\varepsilon_{11})$) (· · · ·) stress/strain curves are displayed for comparison

followed by the material in each experiment (e.g. *Figure 15*). It is now the object of this section to separate the respective influence of strain and strain-rate in order to determine the effective stress/strain curve for a fixed reference strain-rate $\dot{\varepsilon}_R$ (arbitrarily chosen as $5\times10^{-3}\,s^{-1}$). This curve is determined by the following equation:

$$\sigma_e(\varepsilon_e, \dot{\varepsilon}_R)=\sigma_e(\varepsilon_e, \dot{\varepsilon}_e)\left[\frac{\dot{\varepsilon}_R}{\dot{\varepsilon}_e}\right]^{\bar{m}} \quad (14)$$

This transformation was applied to the whole set of effective stress/strain curves obtained for all the temperatures investigated. In *Figure 18*, it is applied to tests performed at 20°C, at five different strain rates (dotted lines), the average curve is displayed as a solid line. The average curves likewise obtained for all the temperatures investigated are shown in *Figure 19*. It is important to note that the maximum discrepancy between the curves corrected was always <7%. This discrepancy was similar for all the temperatures tested.

Analytical determination of the constitutive relations

Although the experimental effective stress/strain relation derived previously describes with good precision the intrinsic plastic response of the material, it is more convenient for many applications to use an analytical equation rather than an array of curves. Such an equation will now be proposed.

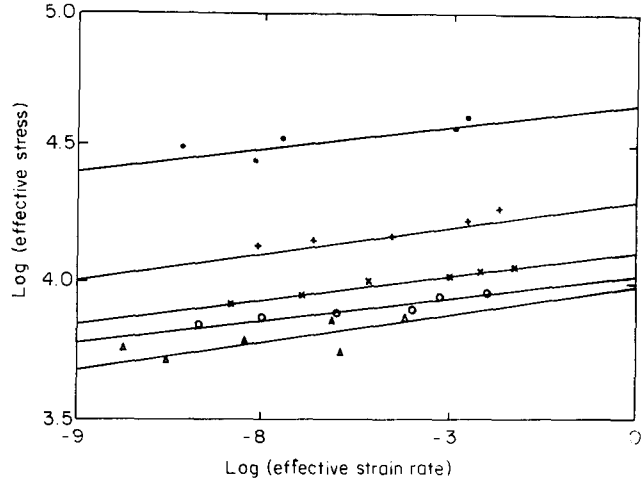

Figure 16 Influence of the effective strain rate on the effective stress at 20°C for various values of the effective strain ε and strain-rate sensitivity coefficient m. ●, $\varepsilon=1.00$, $m=0.029$; +, $\varepsilon=0.75$, $m=0.033$; ×, $\varepsilon=0.50$, $m=0.030$; ○, $\varepsilon=0.25$, $m=0.030$; △, $\varepsilon=0.04$, $m=0.039$

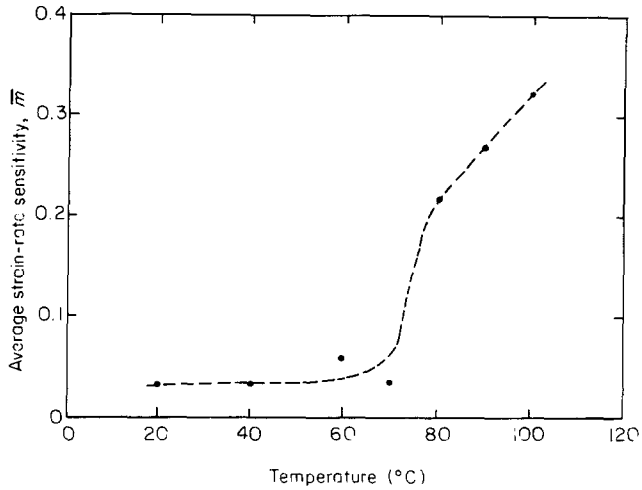

Figure 17 Determination of the average strain-rate sensitivity coefficient, $\bar{m}$, as a function of temperature

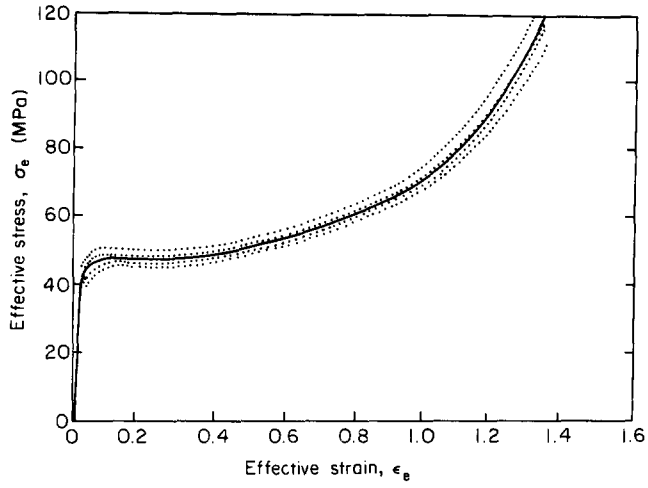

Figure 18 Effective stress/strain behaviour at the reference strain rate of $\dot{\varepsilon}_e = 5 \times 10^{-3}\,s^{-1}$ (——), obtained at 20°C from five different tests (····)

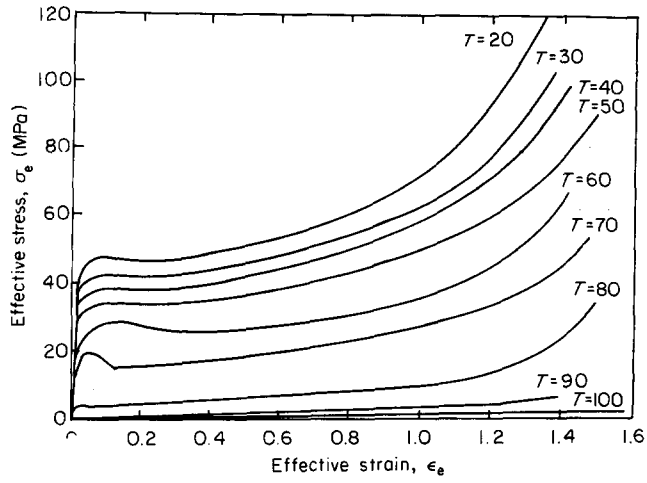

Figure 19 Effective stress/strain curves of PET obtained at different temperatures between 20°C and 100°C for the reference strain rate of $\dot{\varepsilon}_e = 5 \times 10^{-3}\,s^{-1}$

Two types of constitutive relations have been developed in the literature for polymers, which separate the strain and strain-rate variables through multiplicative[4,7] or additive[21,22] forms. In the present work, the multiplicative model appeared to be more accurate. We have used a particular equation which had been successfully applied before to various polymeric materials[5–7,19]:

$$\sigma_e(\varepsilon_e, \dot{\varepsilon}_e) = K Y(\varepsilon_e) \exp(H\varepsilon_e^2) \left[\frac{\dot{\varepsilon}_e}{\dot{\varepsilon}_0}\right]^m \qquad (15)$$

where K is a scaling factor, $Y(\varepsilon_e)$ is a yield transient function which is equal to 0 at $\varepsilon_e = 0$ and tends toward 1 shortly after the plastic regime is reached, H is the hardening coefficient and $\dot{\varepsilon}_0$ is a normalizing strain rate.

In the case of the PET films deformed between 20 and 100°C, the adjustable coefficients of the above equation were determined by the following method:

- $\dot{\varepsilon}_0$ was conventionally fixed at a value of $1\,s^{-1}$;
- m was set equal to the average strain-rate sensitivity coefficient, $\bar{m}$;
- H was obtained from the slope of the experimental $\ln(\sigma_e)$ *versus* $\ln(\dot{\varepsilon}_e)$ which becomes a straight line in the range of large strain since $\ln(\sigma_e)$ reduces to $\ln(K) + H\varepsilon_e^2 + m\ln(\dot{\varepsilon}_e/\dot{\varepsilon}_0)$ as soon as $Y(\varepsilon_e)$ has reached unity;
- K was derived from the ordinate intercept of the above straight line at zero strain, equal to $\ln(K) + m\ln(\dot{\varepsilon}_e/\dot{\varepsilon}_0)$.

Concerning the yield function $Y(\varepsilon_e)$, it should ideally take into account both the initial high modulus portion of the $\sigma_e(\varepsilon_e)$ curve, and the stress drop observed at yield. Unfortunately, it was shown in a previous work[22] that this transient behaviour results from the dynamic multiplication of micro shear domains in the glassy structure and, consequently, that the corresponding dependence of σ_e on ε_e cannot be expressed readily in an integrated form. Furthermore, it is clear in *Figure 19* that for PET films, the amplitude of the yield drop is relatively small (except at 60°C and 70°C where it is unexpectedly larger). Consequently, it was chosen here to neglect the strain softening effect and to approximate the $Y(\varepsilon_e)$ by the following expression derived previously[5] for several semicrystalline polymers (PE, PP, PTFE, etc.) free from yield drop:

$$Y(\varepsilon) = [1 - \exp(-w\varepsilon_e)] \qquad (16)$$

where w is a fitting coefficient numerically calculated from the following expression:

$$2H\varepsilon_c + w + 1 = \exp(w\varepsilon_c) \qquad (17)$$

where ε_c is the effective strain at the Considère's point[24].

The values of K, H, m and w thus obtained are listed in *Table 1*.

The constitutive equation being complete, the modelled stress/strain curves are finally plotted in the investigated range of temperatures (*Figure 20*). It is interesting to note that they describe with fairly good precision the experimental behaviour of the material, including the elasto-viscoplastic response at room temperature and the very soft rubber-like curves in the vicinity of the glass transition temperature.

DISCUSSION

Although it was shown that the procedure described in the previous section is well adapted to the case of amorphous PET films for values of the stretching ratio not greater than $\lambda \simeq 3$, its applicability to semicrystalline polymers and to very high strains is still questionable. In the case of semicrystalline polymers above T_g, the quantitative analysis of the propagation of the neck requires more precautions than for PET, since the films exhibit a non-negligible creep within the unnecked region under the effect of the plateau stress. Therefore,

Table 1 Parameters of the constitutive relation of the PET film (equation (14)) at different temperatures

T (°C)	K (MPa)	w	H	$\bar{m}$
20	50.7	65	0.53	0.030
30	47.1	65	0.48	0.032
40	43.3	65	0.48	0.034
50	38.6	62	0.44	0.035
60	27.5	50	0.49	0.037
70	22.0	30	0.51	0.058
80	16.1	13	0.68	0.216
90	7.9	4	0.56	0.270
100	5.8	4	0.31	0.325

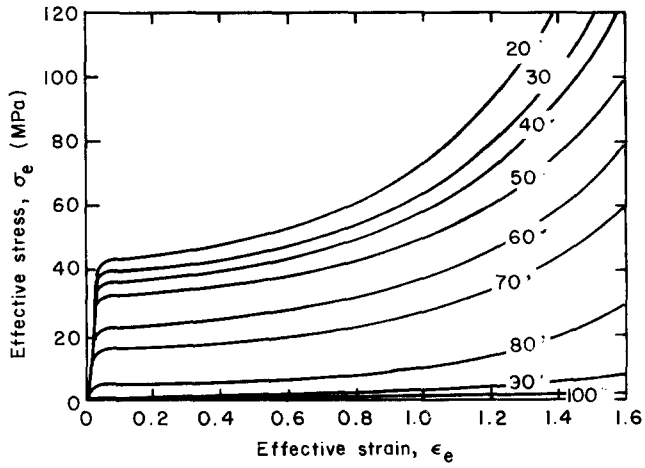

Figure 20 Effective stress/strain curves obtained with the parameters in *Table 1*

the model utilized for the determination of $\dot{\varepsilon}_{11}$ (equation (7)) should be slightly corrected to take the creep effect into consideration. Also, for extremely high strains, it is no longer possible to assume that the film remains isotropic because of the chain orientation induced by the deformation. Instead, it should be useful to replace the original flow theory by a more complex approach taking these anisotropy effects into consideration. Several research teams are currently working on the latter problem, including one in this laboratory[23]. Therefore, it can be reasonably envisaged that the applicability of the testing method developed in this work will be extended beyond its present limits.

Despite the previous difficulties, it is very interesting to derive a constitutive equation that can be easily introduced in a computer code (using a finite element scheme, for example) in order to predict the stress/strain-rate path followed by a polymeric material subjected to a solid-state forming process such as hydrostatic extrusion, biaxial stretching, close-die forging or thermoforming. The optimization of these industrial processes can thus be done through adequate simulations based on the plastic behaviour determined by the present method, employing only thin film specimens.

CONCLUSIONS

Plane-strain stretching tests were performed with films of poly(ethylene terephthalate) at different temperatures and stretching rates. The plastic behaviour of the material was characterized by: (i) the overall stress/stretch curve recorded during the test, (ii) the local strain distribution within the film specimens and (iii) the propagation kinetics of the neck (when such a plastic instability occurs). On the basis of reasonable assumptions (including the applicability of the J_2 flow theory), it was shown that these data can be readily processed in order to derive the effective stress/strain/strain-rate equation of the material which represents the constitutive plastic behaviour under pure uniaxial loading even beyond the necking point. It was found that the PET tested exhibits a gradual elastic–plastic transition at yield, followed by a long and progressive hardening stage while strain is increased. The testing method is applicable in principle to any ductile polymeric material provided the basic assumptions are verified. It is particularly recommended for the mechanical characterization of polymer thin films with a single solid phase (extruded or evaporated thin films, microtomed slices of massive pieces, etc.). It is also suggested for the characterization of new polymer grades, when the material is scarce.

ACKNOWLEDGEMENTS

The authors are grateful to the Mexican Council for Science and Technology (CONACYT) for the award of a graduate fellowship (1982–1986) to one of them (A.M.-L.). They are also grateful to Professor K. W. Neale of the University of Sherbrooke (Canada) for valuable discussions and the granting of a postdoctoral fellowship to A.M.-L.

REFERENCES

1 Strenstein, S. S. and Ongchin, L. *Am. Chem. Soc. Polym. Prepr.* 1969, **10**, 117
2 Hope, P. S., Ward, I. M. and Gibson, A. G. *J. Mater. Sci.* 1980, **15**, 2207
3 Brown, N. in 'Failure of Plastics' (Eds W. Brostow and R. D. Corneliussen), Hanser, Munich, 1986, p. 98
4 G'Sell, C. and Jonas, J. J. *J. Mater. Sci.* 1979, **14**, 583
5 G'sell, C. *Rev. Phys. Appl.* 1988, **23**, 1985
6 G'sell, C. 'Plastic Deformation of Amorphous and Semi-Crystalline Materials' (Eds B. Escaig and C. G'Sell), Les Editions de Physique, Les Ulis, France, 1982
7 G'Sell, C. M., Marquez-Lucero, A., Gilormini, P. and Jonas, J. J. *Acta Metall.* 1985, **33**, 759
8 G'Sell, C., Hiver, J. M., Dahoun, A. and Souahi, A. *J. Mater. Sci.* 1992, **27**, 5031
9 Bridgman, P. W. 'Studies in Large Plastic Flow and Fracture', Harvard University Press, Cambridge, MA, 1964, p. 9
10 Pereira, J. R. C. and Porter, R. S. *J. Polym. Sci., Polym. Phys. Edn* 1983, **21**, 1133
11 G'Sell, C., Aly-Helal, N. A., Semiatin, S. L. and Jonas, J. J. *Polymer* 1992, **33**, 1244
12 Fager, L. O. and Bassani, J. L. *Int. J. Solids Struct.* 1986, **22**, 1243
13 Hutchinson, J. W. and Neale, K. W. *J. Mech. Phys. Solids* 1983, **31**, 405
14 Engelaere, J. C., Cavrot, J. P. and Rietsch, F. *Eur. Polym. J.* 1979, **16**, 721
15 Marquez-Lucero, A. *Doct. Ing. Thesis*, INPL, Nancy, 1986
16 Neale, K. W. and Tugcu, P. *J. Mech. Phys. Solids* 1985, **33**, 323
17 Argon, A. S., Im, J. and Needleman, A. *Metall. Trans.* 1973, **6a**, 815
18 Norris, D. M. Jr, Moran, B., Scudder, J. K. and Quinones, D. F. *Mech. Phys. Solids* 1978, **26**, 1
19 G'Sell, C., Marquez-Lucero, A., Souahi, A. and Tong, Y. S. In 'Plastic Instability', Presses de l'Ecole des Ponts et Chaussées, Paris, 1985, p. 159
20 Bridgman, P. W. *Trans. Am. Soc. Metals* 1944, **32**, 553
21 Argon, A. S. 'Polymeric Materials', American Society for Metals, Metals Park, OH, 1973, p. 411
22 G'sell, C. and Jonas, J. J. *J. Mater. Sci.* 1981, **16**, 1956
23 Dahoun, A., G'Sell, C., Philippe, M. J. and Esling, C. in 'Deformation, Yield and Fracture of Polymers', Plastic and Rubber Institute, London, 1991, p. 68
24 Considère, A. *Ann. Ponts Chausseés*, 1885, **9**, 574